Reductant-dependent None-Partial-Complete Degradation of Block Copolymer Disulfide Crosslinked Nanoassemblies

Geun-woo Jin and Younsoo Bae*

Department of Pharmaceutical Sciences, College of Pharmacy, University of Kentucky, Lexington, KY 40536, United States.

ARTICLE INFO

ABSTRACT

Disulfide crosslinked nanoassemblies (ssCNAs) were characterized in this study to assess their reductant-dependent degradation patterns for future development of redox-responsive smart nanomaterials in biomedical applications. The nanoassemblies were prepared from poly(ethylene glycol)-poly(aspartate) block copolymers, crosslinked with cystamine through an amidation reaction, generating 25 nm particles that have a disulfide crosslinked core enveloped with a poly(ethylene glycol) shell. ssCNAs remained unexpectedly stable in the presence of glutathione, a natural reductant overexpressing inside cells to cleave disulfide compounds. Further investigation revealed that ssCNAs underwent none, partial, and complete degradation in aqueous solutions at 37 °C for 48 h, depending on the molecular weight (MW), Connolly surface excluded volume (SEV), and charged state (net negative, neutral, and positive) of a reductant. Among six reductants tested, 2-aminoethanethiol (MW = 77.2, SEV = 52.2 $Å^3$, net positive) was the most efficient for complete degradation of ssCNAs in 1 h, whereas another reductant, similar in structure except the charged state, 2-mercaptoethanol (MW = 78.1, SEV = 50.3 $Å^3$, net neutral), took 4 h for complete nanoassembly degradation. These results indicate that degradation patterns of ssCNAs can be fine-tuned in a reductant-dependent manner, providing a better understanding of chemical stability of disulfide-crosslinked nanoassemblies.

INTRODUCTION

Redox-responsive smart nanomaterials have garnered attention in recent chemistry, biology, and engineering fields to develop tools for diagnosis, signaling, imaging, and treatment of human diseases (Lu *et al.,* 2003; Kim *et al.,* 2008; Santra *et al.,* 2011; Wang *et al.,* 2011). Disulfide bond is frequently used to control the shape, size, and stability of such smart nanomaterials in the body (Sauer *et al.,* 2010; Yang *et al.,* 2011). One example is disulfide crosslinked polymer, which can remain stable under an oxidative condition yet degrade in the presence of reducants in vivo, such as plasma thiols, cysteine, glutathione (GSH) (Li *et al.,* 2011; Bacalocostantis *et al.,* 2012; Kato *et al.,* 2012; Koo *et al.,* 2012). Previous studies demonstrated that these disulfide crosslinked polymers were useful to prepare particulate, vesicular, and micellar assemblies, which can act as nanoscale (< 200 nm) carriers that deliver various diagnostic, imaging, and therapeutic

molecules to tumors or other pathological sites (Miyata *et al.,* 2004; Matsumoto *et al.,* 2008; Fan *et al.,* 2010; Son *et al.,* 2010; Won *et al.,* 2011; Shim *et al.,* 2012). These carriers are typically designed to release their payload selectively inside targeted cells where GSH concentrations are about 1,000 times greater (5 ~ 10 mmol/L) than those in plasma (2 ~ 20 μmol/L) (Lin *et al.,* 2006; Peng *et al.,* 2008; Tang *et al.,* 2009; Ellison *et al.,* 2012). Despite potential and growing needs, smart nanomaterials with disulfide bonds often show variable degradation patterns in in vitro and in vivo applications. One possible reason is that multiple thiol compounds (e.g. cysteine, glutamyl-cysteine, and cysteinyl-glycine) are produced in the body during the synthesis, metabolism, and transport of GSH inside cells, while the concentration of each thiol compound varies in whole blood, plasma, and urine (Rusin *et al.,* 2003; Kuśmierek *et al.,* 2006; Kaluzna-Czaplinska *et al.,* 2011). Adding complexity, thiol compounds in vivo can also exist in three forms (free thiols, homodisulfides, and heterodisulfides). Therefore, it becomes critical to rationally design disulfide-modified nanomaterials, and thus triggering their degradation in a controlled manner forvarious in vitro and in vivo applications.

* *Corresponding Author*
Younsoo Bae, Ph.D.
Department of Pharmaceutical Sciences, College of Pharmacy, University of Kentucky 789 South Limestone, Lexington, KY 40536-0596, USA.
Phone: +1-859-323-6649, Fax: +1-859-257-7564

Based on these backgrounds, we have developed block copolymer disulfidecrosslinked nanoassemblies (ssCNAs) as potential redox-responsive carriers for drug and gene delivery. The ssCNAs were synthesized from PEG-p(Asp) block copolymers that were crosslinked with cystamine (Figure 1). This study is focused on elucidating the mechanism by which these ssCNAs dissociate in the presence of various reductants.

MATERIALS AND METHODS

Materials

β-Benzyl L-aspartate (BLA), triphosgene, N, N'-diisopropyl carbodiimide (DIC), 4-(dimethyl amino)pyridine (DMAP), N-hydroxy succinimide (NHS), cystamine, deuterium oxide (D2O), anhydrous tetrahydrofuran (THF), anhydrous hexane, anhydrous dimethyl sulfoxide (DMSO), anhydrous ethyl ether, anhydrous benzene, sodium hydroxide, and reductants (Table 1) were purchased from Sigma-Aldrich (USA). α-Methoxy-ω-amino poly(ethylene glycol) (mPEG-NH2, 5 kDa) was purchased from NOF Corporation (Japan). Cellulose dialysis bags with molecular weight cut off (MWCO) 6 ~ 8 kDa, buffer solutions, and other consumables were purchased from Fisher Scientific (USA).

Synthesis of block copolymers

β-Benzyl L-aspartate N-carboxy anhydride (BLA-NCA) was prepared by reacting BLA with triphosgene (1.3 eq) in dry THF under nitrogen at 45°C as previously reported with slight modification (Lee *et al.*, 2011; Ponta *et al.*, 2011; Scott *et al.*, 2011). After 1 h, the solution was washed with anhydrous hexane, using a glass filters under nitrogen. BLA-NCA was re-dissolved in THF, followed by adding hexane dropwise until the solution turns slightly cloudy.

The solution was put at -20°C overnight for recrystallization. BLA-NCA was collected by vacuum drying.Poly(ethylene glycol)-poly(benzyl L-aspartate) (PEG-PBLA) was then synthesized by ring-opening polymerization of BLA-NCA, using mPEG-NH2 as a macro initiator. The number of the aspartate repeating unit was determined by the mixing molar ratio between BLA-NCA and mPEG-NH2. In this study, we synthesized PEG-PBLA with 40 aspartate units. Polymerization was carried out at 40°C in DMSO for 2 days. PEG-PBLA was precipitated in ether and collected by freeze drying from benzene. PEG-PBLA was converted to poly(ethylene glycol)-poly(aspartate) [PEG-p(Asp)] block copolymers by using 0.5N NaOH.

Synthesis of disulfide crosslinked nanoassemblies (ssCNAs)

Disulfide cross-linked nanoassemblies (ssCNAs) were synthesized by cross-linking PEG-p(Asp) with cystamine. PEG-p(Asp) was dissolved in dry DMSO at 100 mg/mL and mixed with DIC, NHS, and DMAP at 4:4:0.2 molar ratio with respect to the number of aspartate groups per polymer chain. After stirring for 1 h, cross-linking reaction was conducted by adding cystamine to the solution at room temperature. The degree of cross-linking was controlled by adjusting the ratio between two amino groups of cystamine and the carboxyl groups of PEG-p(Asp) block copolymers.

The cross-linking reaction was allowed to proceed at room temperature for 3 days. The ssCNAs were precipitated in diethyl ether, followed by further purification through dialysis, centrifugal ultrafiltration (MWCO 100 kDa), and fast protein liquid chromatography (FPLC, AKTA Avant, Superose 12 10/300 GL column, PBS 1×) to obtain final product.

Preliminary particle stability test for ssCNAs in the presence of glutathione

Particle stability of ssCNA was evaluated by incubating the particle (1 mg/mL in PBS, pH 7.4) with 20 mM glutathione (GSH) at 37°C for 48 h. The solutions were stirred gently during incubation.

Comparison of ssCNA Degradation patterns with various reductants

ssCNAs were incubated in PBS (pH 7.4) at 37°C for 48 h with reductants with a different size and charge, which include 3-mercapto-2-methylpropanoic acid (Reductant 1), cysteine (Reductant 2), methyl 2-amino-3-mercaptopropanoate (Reductant 3), 2-mercaptoacetic acid (Reductant 4), 2-mercaptoethanol (Reductant 5), and 2-aminoethanethiol (Reductant 6). Molecular parameters of these reductants are in Table 1. The amount of ssCNAs remaining was determined by GPC peak integration, and shown in percentage with respect to the initial peak area of ssCNA.

RESULTS AND DISCUSSION

Synthesis of ssCNAs

Proton nuclear magnetic resonance (^{1}H-NMR) measurements revealed that the crosslinking yield of ssCNA was 17.5% (Figure 2A). Gel permeation chromatography (GPC) coupled with UV/RI detectors and a static light scattering(SLS) analyzer for absolute molecular weight determination confirmed that ssCNAs were homogeneous and the molecular weight (MW) was approximately 220 kDa, indicating that each ssCNA particle includes twenty three PEG-p(Asp) (MW = 9,600 Da) block copolymer chains (Figure 2B). The particle diameter of ssCNAs was about 25 nm with a narrow distribution, which was determined by dynamic light scattering (DLS) measurements (Figure 2C).

Raw ssCNAs appeared to contain impurities such as unreacted polymer and crosslinkers, which were completely removed by FPLC purification (Figure 3A). Zeta-potential measurements showed that ssCNAs were neural particles (ζ = - 5 mV), although > 80% of carboxyl groups remained unreacted in the core. These results indicate that the PEG shell can shield the charge of the core effectively. (Suh *et al.*, 2002; Dadashzadeh *et al.*, 2010)

Table. 1: Molecular parameters of reductants used in this study. Property computation was performed using CS Chem 3D Pro 11 software.

Reductants	Connolly accessible area ($Å^2$)	Connolly molecular area ($Å^2$)	Connolly solvent excluded volume ($Å^3$)	Molecular weight	Ovality	Principle moment
3-Mercapto-2-methyl propanoic acid	255.81	104.95	77.61	120.17	1.19	152.57
Cysteine	251.74	102.47	75.37	121.16	1.19	150.55
Methyl 2-amino-3-mercaptopropanoate	278.29	116.48	86.24	135.18	1.23	192.67
2-Mercaptoacetic acid	215.02	80.72	54.81	92.12	1.16	42.49
2-Mercaptoethanol	208.26	76.21	50.28	78.13	1.16	17.55
2-Aminoethanethiol	212.22	78.45	52.21	77.15	1.16	18.86
Glutathione (reduced)	539.03	274.09	263.34	307.32	1.48	1483.89
Glutathione (oxidized)	967.03	523.83	465.41	612.63	1.8	4458.9
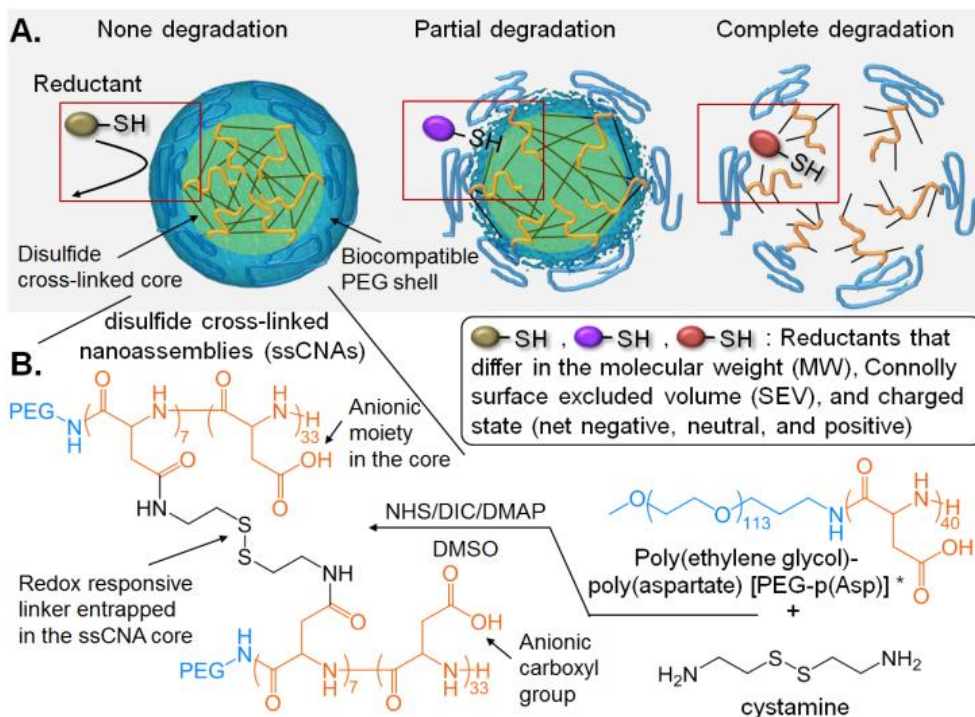
Fig. 1: Disulfide crosslinked nanoassemblies (ssCNAs). (A) Hypothetical mechanism for reductant-dependent degradation patterns. (B) Synthesis of ssCNAs and their block copolymer components.
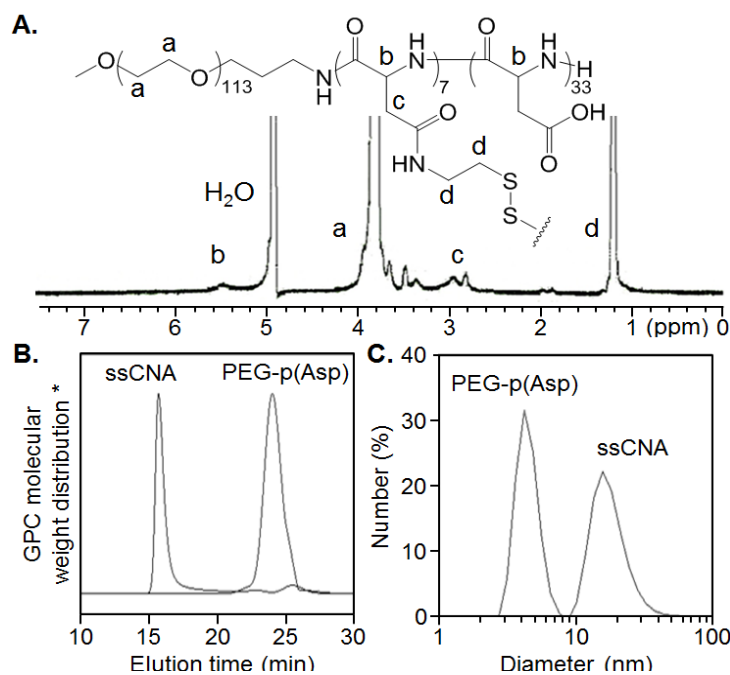
Fig. 2: Characterization of ssCNAs. (A) 1H-NMR spectrum in D2O (500 MHz, Varian). (B) GPC spectra (Shimadzu LC20 equipped with Superose 12 10/300 GL column, PBS 1×, UV/RI/SLS detectors) (C) Dynamic light scattering measurements (Zetasizer Nano ZS, Malvern).
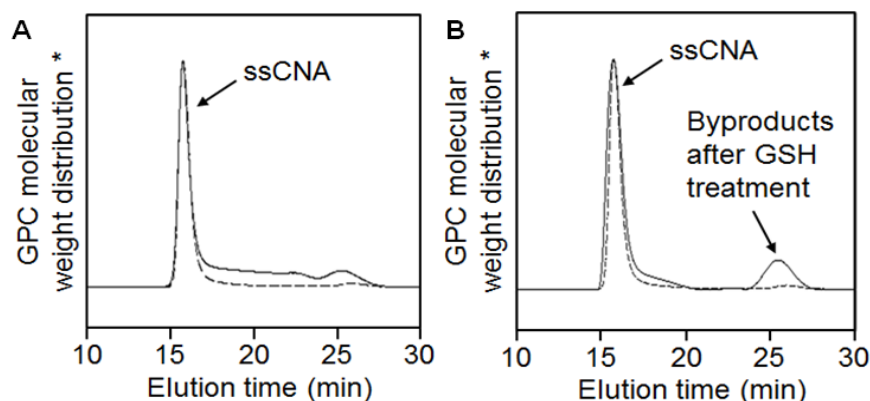
Fig. 3: GPC analysis. GPC spectra of ssCNAs before (solid line) and after (dotted line) FPLC purification (A). GPC spectra of ssCNAs in the presence of GSH. Molecular weight distribution changed before (dotted line) and after (solid line) GSH treatment for 48 h (B). * Normalized by peak height, using an equipped software (LCsolution, Shimadzu).
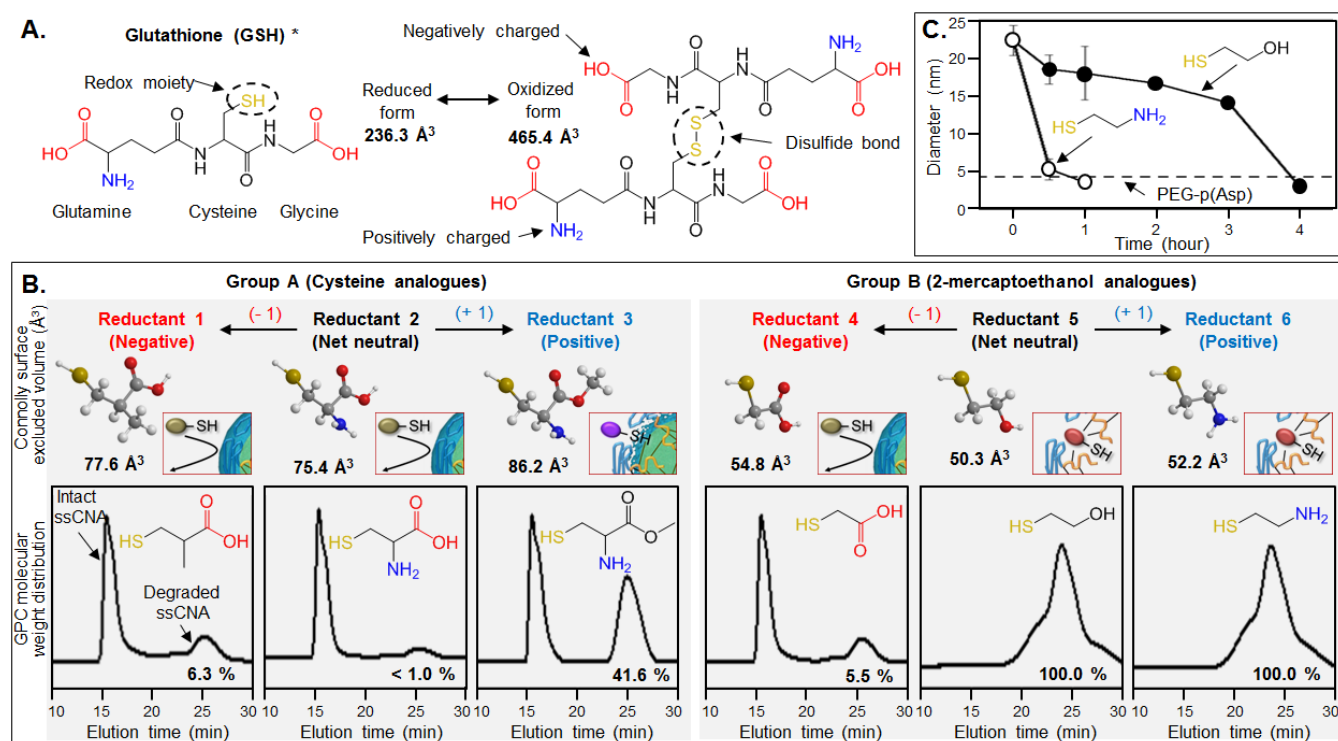

Fig. 4: Reductant-dependent degradation patterns of ssCNAs. (A) Molecular structures of glutathione (GSH) in reduced and oxidized form. GSH caused no ssCNA degradation in our preliminary experiments. (B) Six reductants tested in this study. Molecular size and charge led to none-partial-complete ssCNA degradation. GPC spectra indicate molecular weight distribution, following incubation of ssCNAs with each reductant at 37 °C for 48 h. (C) Degradation profiles of ssCNAs co-incubated with 2-mercaptoethanol (Reductant 5, closed circle) and 2-aminoethanethiol (Reductant 6, open circle). PEG-p(Asp) block copolymer was used as control to determine complete ssCNA degradation by measuring DLS as shown in Figure 2C.

Stability of ssCNAs in the presence of GSH

In our preliminary experiments, ssCNAs (1 mg/mL in PBS, pH 7.4) were incubated with 20 mM of GSH at 37°C for 48h, but no particle degradation was observed (Figure 3B). Our initial speculation was that the crosslinked core of ssCNAs was packed too tightly for GSH to get inside the particle core and degrade the disulfide bonds (Figure 1A). GSH is a bulky reductant comprising cysteine, glutamine, and glycine, producing reduced and oxidized forms in vivo (Figure 4A), and thus, unsuccessful ssCNA degradation might be attributed to the size exclusion effect between GSH molecules and the disulfide crosslinked core of the

particle. In comparison to the cysteine portion of GSH, which typically plays an important role in GSH-mediated disulfide reduction, glutamate and glycine are not directly involved in disulfide degradation while increasing the size of GSH molecule. In addition to steric hindrance, it is also speculated that glutamate and glycine might have induced charge repulsion, hampering the interaction between net negatively charged GSH and ssCNAs that have an anionic core where carboxyl groups of PEG-p(Asp) block copolymers are highly condensed (Figure 1B). These speculations, however, did not explain successful degradation of crosslinked nanoassemblies in the presence of compounds that are greater than

GSH (MW = 307.3, reduced form, and MW = 612.2, oxidized form), such as anticancer drugs [e.g. doxorubicin (MW = 580), 17-N-allylamino-17-demethoxygeldanamycin (MW = 586), and mithramycin-SDK (MW = 1,053)] or fluorescence dyes [e.g. Alexa 488 (MW = 643) and Alexa 680 (MW = 1,150)]. (Lee *et al.,* 2011; Ponta *et al.,* 2011; Scott *et al.,* 2011) Nevertheless, it is still reasonable to surmise that GSH failed to degrade ssCNAs either because the molecular size of GSH was too large to penetrate into the crosslinked core of ssCNAs and react with the disulfide bond, or because the charge repulsion prevented negatively charged GSH from interacting with the anionic core of ssCNAs. We hypothesized that the size and charge of a reductant would play a co-operative role in triggering ssCNA degradation.

Stability of ssCNAs in the presence of various reductants

We further investigated degradation patterns of ssCNAs by using six reductants with different sizes and net charges, which correspond to glutamate (zwitter ions), cysteine (thiol group), and glycine (anionic carboxyl group) portions of GSH, and thus elucidating their effects on particle degradation (Figure 4A). As shown in Figure 4B, the reductants were divided into two groups of cysteine analogues (Group A) and 2-mercaptoethanol analogues (Group B). All reductants in Group A were molecules larger than those in Group B. Each group contained net negative (Reductants 1 and 4: 3-mercapto-2-methylpropanoic acid and 2-mercaptoacetic acid), neutral (Reductants 2 and 5: cysteine and 2-mercaptoethanol), and positive reductants (Reductants 3 and 6: methyl 2-amino-3-mercaptopropanoate and 2-aminoethanethiol). The Connolly surface excluded volume (SEV) of each reductant was smaller (50.3 ~ 86.2 Å^3) than that of GSH (236.3 Å^3, reduced form, and 465.4 Å^3, oxidized form) as shown in Figure 4 (see Table 1 for other molecular parameters). ssCNAs were then incubated with reductants in PBS buffer (pH 7.4) at 37 °C for 48 h. Reductant concentrations were set 20 mM for all experiments. GPC analyses revealed that ssCNA degradation was clearly dependent on a reductant co-incubated with the particle (Figure 4B).

GPC molecular weight distribution patterns indicate that Reductants 1, 2, and 4 caused 6.3 %, < 1.0 %, and 5.5 % ssCNAs degradation, respectively (defined as 'none degradation'). Reductant 3 led to partial degradation, which was statistically significant with respect to intact ssCNA control. Noticeably, Reductants 5 and 6 showed 'complete degradation' at 37 °C in 48 h. ssCNAs incubated with Reductants 2 and 5 indicate that the particle degradation is dependent on the size of a reductant. Reductant 5 (SEV = 50.3 Å^3) degraded ssCNAs completely when larger Reductant 2 (SEV = 75.4 Å^3) induced no particle degradation. Nevertheless, particle degradation patterns cannot be explained either solely by the size of a reductant, as shown in cases of Reductants 3 and 4. Reductant 3 degraded ssCNAs more efficiently than Reductant 4 although Reductant 3 was larger (SEV = 86.2 Å^3) than Reductant 4 (SEV = 54.8 Å^3). In addition, ssCNAs degradation was accelerated with positively charged Reductant 6 in comparison to neutral Reductant 5, indicating that the charge

attraction between a reductant and the negatively charged ssCNAs core would be critical when the size of a reductant is similar. However, it must be emphasized that the charge repulsion between the particles and reductants could not be determined by simply measuring zetapotential of nanoparticles, as the particles used in this study were neutral (ζ = - 5 mV).

These results support our hypothesis that the size and net charge of a reductant may be co-factors that determine ssCNAs degradation in combination. For instance, Reductants 1, 2, and 4 were smaller than GSH, yet they still failed to degrade ssCNAs presumably because they had net negative charges, which could cause charge repulsion between the reductants and ssCNAs, leading to none degradation. It is interesting that Reductant 3 resulted in 'partial degradation' (about 60% of ssCNA remained intact) with statistical significance ($p < 0.01$) in comparison to Reductants 1, 2, and 4. These results suggest that not the presence of an ionizable group but a net charge plays a critical role for a reductant to permeate into the ssCNA core. Reductant 3, the largest molecule among cysteine analogues tested, was initially considered too large to enter the ssCNA core, but its net positive charge seemed to moderately overcome the size exclusion effect, resulting in partial degradation of the particle. Partial ssCNA degradation suggests that the core of ssCNAs might be a mesh-like structure with a pore size close to the SEV of Reductant 3, attracting the positively charged reductant to the anionic particle core to trigger disulfide bond degradation. Oppositely, Reductant 4 could not go into the ssCNA core due to its net negative charge although it was smaller than Reductant 3. Complete particle degradation was achieved only by Reductants 5 and 6. Reductants 5 and 6 were small molecules with no or positive charge, which presumably contributed to effective disulfide bond reduction. It is noted that positively charged Reductant 6 accelerated ssCNA degradation in comparison to neutral Reductant 5, which was determined by time-dependent DLS measurements (Figure 4C). As opposed to negatively charged Reductant 4 and neutral Reductant 5, Reductant 6 with an amino group seemed to interact more effectively with the anionic ssCNA core, and degradethe disulfide bonds entrapped in the particle. These data suggest that the core environment of ssCNAs dramatically affects degradation patterns of polymer nanoassemblies entrapping disulfide bonds, and therefore, reductants should be carefully selected to trigger degradation of the disulfide bonds inside nanoparticles in order to avoid undesirable charge repulsion and size exclusion effects.

CONCLUSIONS

Taken together, our results lead to conclusions that: 1) the molecular size and net charge of a reductant co-operatively affect degradation patterns of disulfide bonds entrapped in a nanoparticle core; 2) none, partial, and complete degradation of disulfide crosslinked nanoassemblies can be achieved in a reductant-dependent manner; 3) ionizable groups entrapped in the nanoparticle core along with the disulfide bonds should be carefully considered for the selection and design of a reductant to

trigger degradation of disulfide crosslinked nanoparticles; and thus 4) degradability of disulfide stabilized nanomaterials should be assessed with not only GSH but also other reductants, considering that various thiol compounds are present in plasma and cells. Our findings in this study, therefore, will contribute to determining optimal conditions for reductant-dependent degradation of nanoparticles for drug and gene delivery, and may lead to the development of novel nanodevices that can degrade multimodally responsive and fine-tunable manners by concurrently engineering host nanomaterials and their guest reductants.

ACKNOWLEDGMENTS

REFERENCES

Bacalocostantis I., Mane V.P., Kang M.S., Goodley A.S., Muro S., and Kofinas P. Effect of Thiol Pendant Conjugates on Plasmid DNA Binding, Release, and Stability of Polymeric Delivery Vectors. *Biomacromolecules* 2012; *5*: 1331-1339.

Dadashzadeh S., Mirahmadi N., Babaei M.H., and Vali A.M. Peritoneal retention of liposomes: Effects of lipid composition, PEG coating and liposome charge. *J Control Release* 2010; *2*: 177-186.

Ellison I., and Richie Jr J.P. Mechanisms of glutathione disulfide efflux from erythrocytes. *Biochem Pharmacol* 2012; *1*: 164-169.

Fan H., Huang J., Li Y., Yu J., and Chen J. Fabrication of reduction-degradable micelle based on disulfide-linked graft copolymer-camptothecin conjugate for enhancing solubility and stability of camptothecin. *Polymer* 2010; *22*: 5107-5114.

Kaluzna-Czaplinska J., Michalska M., and Rynkowski J. Homocysteine level in urine of autistic and healthy children. *Acta biochimica Polonica* 2011; *1*: 31-34.

Kato J., Li Y., Xiao K., Lee J.S., Luo J., Tuscano J.M., O'Donnell R.T., and Lam K.S. Disulfide Cross-Linked Micelles for the Targeted Delivery of Vincristine to B-Cell Lymphoma. *Mol Pharm* 2012; *6*: 1727-1735.

Kim S.H., Jeong J.H., Kim T.-i., Kim S.W., and Bull D.A. VEGF siRNA Delivery System Using Arginine-Grafted Bioreducible Poly(disulfide amine). *Mol Pharm* 2008; *3*: 718-726.

Koo A.N., Min K.H., Lee H.J., Lee S.-U., Kim K., Chan Kwon I., Cho S.H., Jeong S.Y., and Lee S.C. Tumor accumulation and antitumor efficacy of docetaxel-loaded core-shell-corona micelles with shell-specific redox-responsive cross-links. *Biomaterials* 2012; *5*: 1489-1499.

Kuśmierek K., Głowacki R., and Bald E. Analysis of urine for cysteine, cysteinylglycine, and homocysteine by high-performance liquid chromatography. *Anal Bioanal Chem* 2006; *5*: 855-860.

Lee H.J., and Bae Y. Cross-Linked Nanoassemblies from Poly(ethylene glycol)-poly(aspartate) Block Copolymers as Stable Supramolecular Templates for Particulate Drug Delivery. *Biomacromolecules* 2011; *7*: 2686-2696.

Li Y., Xiao K., Luo J., Xiao W., Lee J.S., Gonik A.M., Kato J., Dong T.A., and Lam K.S. Well-defined, reversible disulfide cross-linked micelles for on-demand paclitaxel delivery. *Biomaterials* 2011; *27*: 6633-6645.

Lin C., Zhong Z., Lok M.C., Jiang X., Hennink W.E., Feijen J., and Engbersen J.F.J. Linear poly(amido amine)s with secondary and tertiary amino groups and variable amounts of disulfide linkages: Synthesis and in vitro gene transfer properties. *J Control Release* 2006; *2*: 130-137.

Lu Z.-R., Wang X., Parker D.L., Goodrich K.C., and Buswell H.R. Poly(l-glutamic acid) Gd(III)-DOTA Conjugate with a Degradable Spacer for Magnetic Resonance Imaging. *Bioconjugate Chem* 2003; *4*: 715-719.

Matsumoto S., Christie R.J., Nishiyama N., Miyata K., Ishii A., Oba M., Koyama H., Yamasaki Y., and Kataoka K. Environment-Responsive Block Copolymer Micelles with a Disulfide Cross-Linked Core for Enhanced siRNA Delivery. *Biomacromolecules* 2008; *1*: 119-127.

Miyata K., Kakizawa Y., Nishiyama N., Harada A., Yamasaki Y., Koyama H., and Kataoka K. Block Catiomer Polyplexes with Regulated Densities of Charge and Disulfide Cross-Linking Directed To Enhance Gene Expression. *J Am Chem Soc* 2004; *8*: 2355-2361.

Peng Q., Zhong Z., and Zhuo R. Disulfide Cross-Linked Polyethylenimines (PEI) Prepared via Thiolation of Low Molecular Weight PEI as Highly Efficient Gene Vectors. *Bioconjugate Chem* 2008; *2*: 499-506.

Ponta A., Akter S., and Bae Y. Degradable Cross-Linked Nanoassemblies as Drug Carriers for Heat Shock Protein 90 Inhibitor 17-N-Allylamino-17-demethoxy-geldanamycin. *Pharmaceuticals* 2011; *10*: 1281-1292.

Rusin O., St. Luce N.N., Agbaria R.A., Escobedo J.O., Jiang S., Warner I.M., Dawan F.B., Lian K., and Strongin R.M. Visual Detection of Cysteine and Homocysteine. *J Am Chem Soc* 2003; *2*: 438-439.

Santra S., Kaittanis C., Santiesteban O.J., and Perez J.M. Cell-Specific, Activatable, and Theranostic Prodrug for Dual-Targeted Cancer Imaging and Therapy. *J Am Chem Soc* 2011; *41*: 16680-16688.

Sauer A.M., Schlossbauer A., Ruthardt N., Cauda V., Bein T., and Bräuchle C. Role of Endosomal Escape for Disulfide-Based Drug Delivery from Colloidal Mesoporous Silica Evaluated by Live-Cell Imaging. *Nano Lett* 2010; *9*: 3684-3691.

Scott D., Rohr J., and Bae Y. Nanoparticulate formulations of mithramycin analogs for enhanced cytotoxicity. *Int J Nanomed* 2011; 2757-2767.

Shim M.S., and Kwon Y.J. Stimuli-responsive polymers and nanomaterials for gene delivery and imaging applications. *Adv Drug Deliver Rev* 2012; *11*: 1046-1059.

Son S., Singha K., and Kim W.J. Bioreducible BPEI-SS-PEG-cNGR polymer as a tumor targeted nonviral gene carrier. *Biomaterials* 2010; *24*: 6344-6354.

Suh W., Han S.O., Yu L., and Kim S.W. An angiogenic, endothelial-cell-targeted polymeric gene carrier. *Molecular therapy : the journal of the American Society of Gene Therapy* 2002; *5*: 664-672.

Tang L.-Y., Wang Y.-C., Li Y., Du J.-Z., and Wang J. Shell-Detachable Micelles Based on Disulfide-Linked Block Copolymer As Potential Carrier for Intracellular Drug Delivery. *Bioconjugate Chem* 2009; *6*: 1095-1099.

Wang Y.-C., Wang F., Sun T.-M., and Wang J. Redox-Responsive Nanoparticles from the Single Disulfide Bond-Bridged Block Copolymer as Drug Carriers for Overcoming Multidrug Resistance in Cancer Cells. *Bioconjugate Chem* 2011; *10*: 1939-1945.

Won Y.-W., Kim K.-M., An S.S., Lee M., Ha Y., and Kim Y.-H. Suicide gene therapy using reducible poly (oligo-d-arginine) for the treatment of spinal cord tumors. *Biomaterials* 2011; *36*: 9766-9775.

Yang J.J., Kularatne S.A., Chen X., Low P.S., and Wang E. Characterization of in Vivo Disulfide-Reduction Mediated Drug Release in Mouse Kidneys. *Mol Pharm* 2011; *2*: 310-317.